PHYSICAL REVIEW D **79,** 032002 (2009)

Measurements of time-dependent *CP* asymmetries in $B^0 \to D^{(*)+} D^{(*)-}$ decays

B. Aubert,[1] M. Bona,[1] Y. Karyotakis,[1] J. P. Lees,[1] V. Poireau,[1] E. Prencipe,[1] X. Prudent,[1] V. Tisserand,[1] J. Garra Tico,[2] E. Grauges,[2] L. Lopez,[3a,3b] A. Palano,[3a,3b] M. Pappagallo,[3a,3b] G. Eigen,[4] B. Stugu,[4] L. Sun,[4] G. S. Abrams,[5] M. Battaglia,[5] D. N. Brown,[5] R. N. Cahn,[5] R. G. Jacobsen,[5] L. T. Kerth,[5] Yu. G. Kolomensky,[5] G. Lynch,[5] I. L. Osipenkov,[5] M. T. Ronan,[5] K. Tackmann,[5] T. Tanabe,[5] C. M. Hawkes,[6] N. Soni,[6] A. T. Watson,[6] H. Koch,[7] T. Schroeder,[7] D. Walker,[8] D. J. Asgeirsson,[9] B. G. Fulsom,[9] C. Hearty,[9] T. S. Mattison,[9] J. A. McKenna,[9] M. Barrett,[10] A. Khan,[10] V. E. Blinov,[11] A. D. Bukin,[11] A. R. Buzykaev,[11] V. P. Druzhinin,[11] V. B. Golubev,[11] A. P. Onuchin,[11] S. I. Serednyakov,[11] Yu. I. Skovpen,[11] E. P. Solodov,[11] K. Yu. Todyshev,[11] M. Bondioli,[12] S. Curry,[12] I. Eschrich,[12] D. Kirkby,[12] A. J. Lankford,[12] P. Lund,[12] M. Mandelkern,[12] E. C. Martin,[12] D. P. Stoker,[12] S. Abachi,[13] C. Buchanan,[13] J. W. Gary,[14] F. Liu,[14] O. Long,[14] B. C. Shen,[14,*] G. M. Vitug,[14] Z. Yasin,[14] L. Zhang,[14] V. Sharma,[15] C. Campagnari,[16] T. M. Hong,[16] D. Kovalskyi,[16] M. A. Mazur,[16] J. D. Richman,[16] T. W. Beck,[17] A. M. Eisner,[17] C. J. Flacco,[17] C. A. Heusch,[17] J. Kroseberg,[17] W. S. Lockman,[17] A. J. Martinez,[17] T. Schalk,[17] B. A. Schumm,[17] A. Seiden,[17] M. G. Wilson,[17] L. O. Winstrom,[17] C. H. Cheng,[18] D. A. Doll,[18] B. Echenard,[18] F. Fang,[18] D. G. Hitlin,[18] I. Narsky,[18] T. Piatenko,[18] F. C. Porter,[18] R. Andreassen,[19] G. Mancinelli,[19] B. T. Meadows,[19] K. Mishra,[19] M. D. Sokoloff,[19] P. C. Bloom,[20] W. T. Ford,[20] A. Gaz,[20] J. F. Hirschauer,[20] M. Nagel,[20] U. Nauenberg,[20] J. G. Smith,[20] K. A. Ulmer,[20] S. R. Wagner,[20] R. Ayad,[21,†] A. Soffer,[21,‡] W. H. Toki,[21] R. J. Wilson,[21] D. D. Altenburg,[22] E. Feltresi,[22] A. Hauke,[22] H. Jasper,[22] M. Karbach,[22] J. Merkel,[22] A. Petzold,[22] B. Spaan,[22] K. Wacker,[22] M. J. Kobel,[23] W. F. Mader,[23] R. Nogowski,[23] K. R. Schubert,[23] R. Schwierz,[23] A. Volk,[23] D. Bernard,[24] G. R. Bonneaud,[24] E. Latour,[24] M. Verderi,[24] P. J. Clark,[25] S. Playfer,[25] J. E. Watson,[25] M. Andreotti,[26a,26b] D. Bettoni,[26a] C. Bozzi,[26a] R. Calabrese,[26a,26b] A. Cecchi,[26a,26b] G. Cibinetto,[26a,26b] P. Franchini,[26a,26b] E. Luppi,[26a,26b] M. Negrini,[26a,26b] A. Petrella,[26a,26b] L. Piemontese,[26a] V. Santoro,[26a,26b] R. Baldini-Ferroli,[27] A. Calcaterra,[27] R. de Sangro,[27] G. Finocchiaro,[27] S. Pacetti,[27] P. Patteri,[27] I. M. Peruzzi,[27,§] M. Piccolo,[27] M. Rama,[27] A. Zallo,[27] A. Buzzo,[28a] R. Contri,[28a,28b] M. Lo Vetere,[28a,28b] M. M. Macri,[28a] M. R. Monge,[28a,28b] S. Passaggio,[28a] C. Patrignani,[28a,28b] E. Robutti,[28a] A. Santroni,[28a,28b] S. Tosi,[28a,28b] K. S. Chaisanguanthum,[29] M. Morii,[29] A. Adametz,[30] J. Marks,[30] S. Schenk,[30] U. Uwer,[30] V. Klose,[31] H. M. Lacker,[31] D. J. Bard,[32] P. D. Dauncey,[32] J. A. Nash,[32] M. Tibbetts,[32] P. K. Behera,[33] X. Chai,[33] M. J. Charles,[33] U. Mallik,[33] J. Cochran,[34] H. B. Crawley,[34] L. Dong,[34] W. T. Meyer,[34] S. Prell,[34] E. I. Rosenberg,[34] A. E. Rubin,[34] Y. Y. Gao,[35] A. V. Gritsan,[35] Z. J. Guo,[35] C. K. Lae,[35] N. Arnaud,[26] J. Béquilleux,[26] A. D'Orazio,[26] M. Davier,[26] J. Firmino da Costa,[26] G. Grosdidier,[26] A. Höcker,[26] V. Lepeltier,[26] F. Le Diberder,[26] A. M. Lutz,[26] S. Pruvot,[26] P. Roudeau,[26] M. H. Schune,[26] J. Serrano,[26] V. Sordini,[26,‖] A. Stocchi,[26] G. Wormser,[26] D. J. Lange,[37] D. M. Wright,[37] I. Bingham,[38] J. P. Burke,[38] C. A. Chavez,[38] J. R. Fry,[38] E. Gabathuler,[38] R. Gamet,[38] D. E. Hutchcroft,[38] D. J. Payne,[38] C. Touramanis,[38] A. J. Bevan,[39] C. K. Clarke,[39] K. A. George,[39] F. Di Lodovico,[39] R. Sacco,[39] M. Sigamani,[39] G. Cowan,[40] H. U. Flaecher,[40] D. A. Hopkins,[40] S. Paramesvaran,[40] F. Salvatore,[40] A. C. Wren,[40] D. N. Brown,[41] C. L. Davis,[41] A. G. Denig,[42] M. Fritsch,[42] W. Gradl,[42] G. Schott,[42] K. E. Alwyn,[43] D. Bailey,[43] R. J. Barlow,[43] Y. M. Chia,[43] C. L. Edgar,[43] G. Jackson,[43] G. D. Lafferty,[43] T. J. West,[43] J. I. Yi,[43] J. Anderson,[44] C. Chen,[44] A. Jawahery,[44] D. A. Roberts,[44] G. Simi,[44] J. M. Tuggle,[44] C. Dallapiccola,[45] X. Li,[45] E. Salvati,[45] S. Saremi,[45] R. Cowan,[46] D. Dujmic,[46] P. H. Fisher,[46] G. Sciolla,[46] M. Spitznagel,[46] F. Taylor,[46] R. K. Yamamoto,[46] M. Zhao,[46] P. M. Patel,[47] S. H. Robertson,[47] A. Lazzaro,[48a,48b] V. Lombardo,[48a] F. Palombo,[48a,48b] J. M. Bauer,[49] L. Cremaldi,[49] R. Godang,[49,¶] R. Kroeger,[49] D. A. Sanders,[49] D. J. Summers,[49] H. W. Zhao,[49] M. Simard,[50] P. Taras,[50] F. B. Viaud,[50] H. Nicholson,[51] G. De Nardo,[52a,52b] L. Lista,[52a] D. Monorchio,[52a,52b] G. Onorato,[52a,52b] C. Sciacca,[52a,52b] G. Raven,[53] H. L. Snoek,[53] C. P. Jessop,[54] K. J. Knoepfel,[54] J. M. LoSecco,[54] W. F. Wang,[54] G. Benelli,[55] L. A. Corwin,[55] K. Honscheid,[55] H. Kagan,[55] R. Kass,[55] J. P. Morris,[55] A. M. Rahimi,[55] J. J. Regensburger,[55] S. J. Sekula,[55] Q. K. Wong,[55] N. L. Blount,[56] J. Brau,[56] R. Frey,[56] O. Igonkina,[56] J. A. Kolb,[56] M. Lu,[56] R. Rahmat,[56] N. B. Sinev,[56] D. Strom,[56] J. Strube,[56] E. Torrence,[56] G. Castelli,[57a,57b] N. Gagliardi,[57a,57b] M. Margoni,[57a,57b] M. Morandin,[57a] M. Posocco,[57a] M. Rotondo,[57a] F. Simonetto,[57a,57b] R. Stroili,[57a,57b] C. Voci,[57a,57b] P. del Amo Sanchez,[58] E. Ben-Haim,[58] H. Briand,[58] G. Calderini,[58] J. Chauveau,[58] P. David,[58] L. Del Buono,[58] O. Hamon,[58] Ph. Leruste,[58] J. Ocariz,[58] A. Perez,[58] J. Prendki,[58] S. Sitt,[58] L. Gladney,[59] M. Biasini,[60a,60b] R. Covarelli,[60a,60b] E. Manoni,[60a,60b] C. Angelini,[61a,61b] G. Batignani,[61a,61b] S. Bettarini,[61a,61b] M. Carpinelli,[61a,61b,**] A. Cervelli,[61a,61b] F. Forti,[61a,61b] M. A. Giorgi,[61a,61b] A. Lusiani,[61a,61c] G. Marchiori,[61a,61b] M. Morganti,[61a,61b] N. Neri,[61a,61b] E. Paoloni,[61a,61b] G. Rizzo,[61a,61b] J. J. Walsh,[61a] D. Lopes Pegna,[62] C. Lu,[62] J. Olsen,[62] A. J. S. Smith,[62] A. V. Telnov,[62] F. Anulli,[63a] E. Baracchini,[63a,63b] G. Cavoto,[63a] D. del Re,[63a,63b] E. Di Marco,[63a,63b] R. Faccini,[63a,63b] F. Ferrarotto,[63a] F. Ferroni,[63a,63b] M. Gaspero,[63a,63b] P. D. Jackson,[63a] L. Li Gioi,[63a] M. A. Mazzoni,[63a] S. Morganti,[63a]

G. Piredda,[63a] F. Polci,[63a,63b] F. Renga,[63a,63b] C. Voena,[63a] M. Ebert,[64] T. Hartmann,[64] H. Schröder,[64] R. Waldi,[64] T. Adye,[65] B. Franek,[65] E. O. Olaiya,[65] F. F. Wilson,[65] S. Emery,[66] M. Escalier,[66] L. Esteve,[66] S. F. Ganzhur,[66] G. Hamel de Monchenault,[66] W. Kozanecki,[66] G. Vasseur,[66] Ch. Yèche,[66] M. Zito,[66] X. R. Chen,[67] H. Liu,[67] W. Park,[67] M. V. Purohit,[67] R. M. White,[67] J. R. Wilson,[67] M. T. Allen,[68] D. Aston,[68] R. Bartoldus,[68] P. Bechtle,[68] J. F. Benitez,[68] R. Cenci,[68] J. P. Coleman,[68] M. R. Convery,[68] J. C. Dingfelder,[68] J. Dorfan,[68] G. P. Dubois-Felsmann,[68] W. Dunwoodie,[68] R. C. Field,[68] A. M. Gabareen,[68] S. J. Gowdy,[68] M. T. Graham,[68] P. Grenier,[68] C. Hast,[68] W. R. Innes,[68] J. Kaminski,[68] M. H. Kelsey,[68] H. Kim,[68] P. Kim,[68] M. L. Kocian,[68] D. W. G. S. Leith,[68] S. Li,[68] B. Lindquist,[68] S. Luitz,[68] V. Luth,[68] H. L. Lynch,[68] D. B. MacFarlane,[68] H. Marsiske,[68] R. Messner,[68] D. R. Muller,[68] H. Neal,[68] S. Nelson,[68] C. P. O'Grady,[68] I. Ofte,[68] A. Perazzo,[68] M. Perl,[68] B. N. Ratcliff,[68] A. Roodman,[68] A. A. Salnikov,[68] R. H. Schindler,[68] J. Schwiening,[68] A. Snyder,[68] D. Su,[68] M. K. Sullivan,[68] K. Suzuki,[68] S. K. Swain,[68] J. M. Thompson,[68] J. Va'vra,[68] A. P. Wagner,[68] M. Weaver,[68] C. A. West,[68] W. J. Wisniewski,[68] M. Wittgen,[68] D. H. Wright,[68] H. W. Wulsin,[68] A. K. Yarritu,[68] K. Yi,[68] C. C. Young,[68] V. Ziegler,[68] P. R. Burchat,[69] A. J. Edwards,[69] S. A. Majewski,[69] T. S. Miyashita,[69] B. A. Petersen,[69] L. Wilden,[69] S. Ahmed,[70] M. S. Alam,[70] J. A. Ernst,[70] B. Pan,[70] M. A. Saeed,[70] S. B. Zain,[70] S. M. Spanier,[71] B. J. Wogsland,[71] R. Eckmann,[72] J. L. Ritchie,[72] A. M. Ruland,[72] C. J. Schilling,[72] R. F. Schwitters,[72] B. W. Drummond,[73] J. M. Izen,[73] X. C. Lou,[73] F. Bianchi,[74a,74b] D. Gamba,[74a,74b] M. Pelliccioni,[74a,74b] M. Bomben,[75a,75b] L. Bosisio,[75a,75b] C. Cartaro,[75a,75b] G. Della Ricca,[75a,75b] L. Lanceri,[75a,75b] L. Vitale,[75a,75b] V. Azzolini,[76] N. Lopez-March,[76] F. Martinez-Vidal,[76] D. A. Milanes,[76] A. Oyanguren,[76] J. Albert,[77] Sw. Banerjee,[77] B. Bhuyan,[77] H. H. F. Choi,[77] K. Hamano,[77] R. Kowalewski,[77] M. J. Lewczuk,[77] I. M. Nugent,[77] J. M. Roney,[77] R. J. Sobie,[77] T. J. Gershon,[78] P. F. Harrison,[78] J. Ilic,[78] T. E. Latham,[78] G. B. Mohanty,[78] H. R. Band,[79] X. Chen,[79] S. Dasu,[79] K. T. Flood,[79] Y. Pan,[79] M. Pierini,[79] R. Prepost,[79] C. O. Vuosalo,[79] and S. L. Wu[79]

(*BABAR* Collaboration)

[1]*Laboratoire de Physique des Particules, IN2P3/CNRS et Université de Savoie, F-74941 Annecy-Le-Vieux, France*
[2]*Universitat de Barcelona, Facultat de Fisica, Departament ECM, E-08028 Barcelona, Spain*
[3a]*INFN Sezione di Bari, I-70126 Bari, Italy;*
[3b]*Dipartmento di Fisica, Università di Bari, I-70126 Bari, Italy*
[4]*University of Bergen, Institute of Physics, N-5007 Bergen, Norway*
[5]*Lawrence Berkeley National Laboratory and University of California, Berkeley, California 94720, USA*
[6]*University of Birmingham, Birmingham, B15 2TT, United Kingdom*
[7]*Ruhr Universität Bochum, Institut für Experimentalphysik 1, D-44780 Bochum, Germany*
[8]*University of Bristol, Bristol BS8 1TL, United Kingdom*
[9]*University of British Columbia, Vancouver, British Columbia, Canada V6T 1Z1*
[10]*Brunel University, Uxbridge, Middlesex UB8 3PH, United Kingdom*
[11]*Budker Institute of Nuclear Physics, Novosibirsk 630090, Russia*
[12]*University of California at Irvine, Irvine, California 92697, USA*
[13]*University of California at Los Angeles, Los Angeles, California 90024, USA*
[14]*University of California at Riverside, Riverside, California 92521, USA*
[15]*University of California at San Diego, La Jolla, California 92093, USA*
[16]*University of California at Santa Barbara, Santa Barbara, California 93106, USA*
[17]*University of California at Santa Cruz, Institute for Particle Physics, Santa Cruz, California 95064, USA*
[18]*California Institute of Technology, Pasadena, California 91125, USA*
[19]*University of Cincinnati, Cincinnati, Ohio 45221, USA*
[20]*University of Colorado, Boulder, Colorado 80309, USA*
[21]*Colorado State University, Fort Collins, Colorado 80523, USA*
[22]*Technische Universität Dortmund, Fakultät Physik, D-44221 Dortmund, Germany*
[23]*Technische Universität Dresden, Institut für Kern- und Teilchenphysik, D-01062 Dresden, Germany*
[24]*Laboratoire Leprince-Ringuet, CNRS/IN2P3, Ecole Polytechnique, F-91128 Palaiseau, France*
[25]*University of Edinburgh, Edinburgh EH9 3JZ, United Kingdom*
[26a]*INFN Sezione di Ferrara, I-44100 Ferrara, Italy;*
[26b]*Dipartimento di Fisica, Università di Ferrara, I-44100 Ferrara, Italy;*
[27]*INFN Laboratori Nazionali di Frascati, I-00044 Frascati, Italy*
[28a]*INFN Sezione di Genova, I-16146 Genova, Italy;*
[28b]*Dipartimento di Fisica, Università di Genova, I-16146 Genova, Italy*
[29]*Harvard University, Cambridge, Massachusetts 02138, USA*
[30]*Universität Heidelberg, Physikalisches Institut, Philosophenweg 12, D-69120 Heidelberg, Germany*

[31]*Humboldt-Universität zu Berlin, Institut für Physik, Newtonstr. 15, D-12489 Berlin, Germany*
[32]*Imperial College London, London, SW7 2AZ, United Kingdom*
[33]*University of Iowa, Iowa City, Iowa 52242, USA*
[34]*Iowa State University, Ames, Iowa 50011-3160, USA*
[35]*Johns Hopkins University, Baltimore, Maryland 21218, USA*
[26]*Laboratoire de l'Accélérateur Linéaire, IN2P3/CNRS et Université Paris-Sud 11, Centre Scientifique d'Orsay, B. P. 34, F-91898 Orsay Cedex, France*
[37]*Lawrence Livermore National Laboratory, Livermore, California 94550, USA*
[38]*University of Liverpool, Liverpool L69 7ZE, United Kingdom*
[39]*Queen Mary, University of London, London, E1 4NS, United Kingdom*
[40]*University of London, Royal Holloway and Bedford New College, Egham, Surrey TW20 0EX, United Kingdom*
[41]*University of Louisville, Louisville, Kentucky 40292, USA*
[42]*Johannes Gutenberg-Universität Mainz, Institut für Kernphysik, D-55099 Mainz, Germany*
[43]*University of Manchester, Manchester M13 9PL, United Kingdom*
[44]*University of Maryland, College Park, Maryland 20742, USA*
[45]*University of Massachusetts, Amherst, Massachusetts 01003, USA*
[46]*Massachusetts Institute of Technology, Laboratory for Nuclear Science, Cambridge, Massachusetts 02139, USA*
[47]*McGill University, Montréal, Québec, Canada H3A 2T8*
[48a]*INFN Sezione di Milano, I-20133 Milano, Italy*
[48b]*Dipartimento di Fisica, Università di Milano, I-20133 Milano, Italy*
[49]*University of Mississippi, University, Mississippi 38677, USA*
[50]*Université de Montréal, Physique des Particules, Montréal, Québec, Canada H3C 3J7*
[51]*Mount Holyoke College, South Hadley, Massachusetts 01075, USA*
[52a]*INFN Sezione di Napoli, I-80126 Napoli, Italy;*
[52b]*Dipartimento di Scienze Fisiche, Università di Napoli Federico II, I-80126 Napoli, Italy*
[53]*NIKHEF, National Institute for Nuclear Physics and High Energy Physics, NL-1009 DB Amsterdam, The Netherlands*
[54]*University of Notre Dame, Notre Dame, Indiana 46556, USA*
[55]*Ohio State University, Columbus, Ohio 43210, USA*
[56]*University of Oregon, Eugene, Oregon 97403, USA*
[57a]*INFN Sezione di Padova, I-35131 Padova, Italy;*
[57b]*Dipartimento di Fisica, Università di Padova, I-35131 Padova, Italy*
[58]*Laboratoire de Physique Nucléaire et de Hautes Energies, IN2P3/CNRS, Université Pierre et Marie Curie-Paris6, Université Denis Diderot-Paris7, F-75252 Paris, France*
[59]*University of Pennsylvania, Philadelphia, Pennsylvania 19104, USA*
[60a]*INFN Sezione di Perugia, I-06100 Perugia, Italy;*
[60b]*Dipartimento di Fisica, Università di Perugia, I-06100 Perugia, Italy*
[61a]*INFN Sezione di Pisa, I-56127 Pisa, Italy;*
[61b]*Dipartimento di Fisica, Università di Pisa, I-56127 Pisa, Italy;*
[61c]*Scuola Normale Superiore di Pisa, I-56127 Pisa, Italy*
[62]*Princeton University, Princeton, New Jersey 08544, USA*
[63a]*INFN Sezione di Roma, I-00185 Roma, Italy*
[63b]*Dipartimento di Fisica, Università di Roma La Sapienza, I-00185 Roma, Italy*
[64]*Universität Rostock, D-18051 Rostock, Germany*
[65]*Rutherford Appleton Laboratory, Chilton, Didcot, Oxon, OX11 0QX, United Kingdom*
[66]*CEA, Irfu, SPP, Centre de Saclay, F-91191 Gif-sur-Yvette, France*
[67]*University of South Carolina, Columbia, South Carolina 29208, USA*
[68]*Stanford Linear Accelerator Center, Stanford, California 94309, USA*
[69]*Stanford University, Stanford, California 94305-4060, USA*
[70]*State University of New York, Albany, New York 12222, USA*
[71]*University of Tennessee, Knoxville, Tennessee 37996, USA*
[72]*University of Texas at Austin, Austin, Texas 78712, USA*

[*]Deceased.
[†]Now at Temple University, Philadelphia, Pennsylvania 19122, USA.
[‡]Now at Tel Aviv University, Tel Aviv, 69978, Israel.
[§]Also with Università di Perugia, Dipartimento di Fisica, Perugia, Italy.
[‖]Also with Università di Roma La Sapienza, I-00185 Roma, Italy.
[¶]Now at University of South Alabama, Mobile, Alabama 36688, USA.
[**]Also with Università di Sassari, Sassari, Italy.

[73]*University of Texas at Dallas, Richardson, Texas 75083, USA*
[74a]*INFN Sezione di Torino, I-10125 Torino, Italy*
[74b]*Dipartimento di Fisica Sperimentale, Università di Torino, I-10125 Torino, Italy*
[75a]*INFN Sezione di Trieste, I-34127 Trieste, Italy*
[75b]*Dipartimento di Fisica, Università di Trieste, I-34127 Trieste, Italy*
[76]*IFIC, Universitat de Valencia-CSIC, E-46071 Valencia, Spain*
[77]*University of Victoria, Victoria, British Columbia, Canada V8W 3P6*
[78]*Department of Physics, University of Warwick, Coventry CV4 7AL, United Kingdom*
[79]*University of Wisconsin, Madison, Wisconsin 53706, USA*
(Received 14 August 2008; published 9 February 2009)

We present new measurements of time-dependent *CP* asymmetries for $B^0 \to D^{(*)+}D^{(*)-}$ decays using $(467 \pm 5) \times 10^6$ $B\bar{B}$ pairs collected with the *BABAR* detector located at the PEP-II *B* Factory at the Stanford Linear Accelerator Center. We determine the *CP*-odd fraction of the $B^0 \to D^{*+}D^{*-}$ decays to be $R_\perp = 0.158 \pm 0.028 \pm 0.006$ and find *CP* asymmetry parameters $S_+ = -0.76 \pm 0.16 \pm 0.04$ and $C_+ = +0.00 \pm 0.12 \pm 0.02$ for the *CP*-even component of this decay and $S_\perp = -1.80 \pm 0.70 \pm 0.16$ and $C_\perp = +0.41 \pm 0.49 \pm 0.08$ for the *CP*-odd component. We measure $S = -0.63 \pm 0.36 \pm 0.05$ and $C = -0.07 \pm 0.23 \pm 0.03$ for $B^0 \to D^+D^-$, $S = -0.62 \pm 0.21 \pm 0.03$ and $C = +0.08 \pm 0.17 \pm 0.04$ for $B^0 \to D^{*+}D^-$, and $S = -0.73 \pm 0.23 \pm 0.05$ and $C = +0.00 \pm 0.17 \pm 0.03$ for $B^0 \to D^+D^{*-}$. For the $B^0 \to D^{*\pm}D^{\mp}$ decays, we also determine the *CP*-violating asymmetry $\mathcal{A} = +0.008 \pm 0.048 \pm 0.013$. In each case, the first uncertainty is statistical and the second is systematic. The measured values for the asymmetries are all consistent with the standard model.

DOI: 10.1103/PhysRevD.79.032002 PACS numbers: 13.25.Hw, 11.30.Er, 12.15.Hh

I. INTRODUCTION

In the standard model (SM), *CP* violation is described by the Cabibbo-Kobayashi-Maskawa (CKM) quark mixing matrix, *V* [1,2]. In particular, an irreducible complex phase in the 3×3 mixing matrix is the source of all SM *CP* violation. Both the *BABAR* [3] and Belle [4] collaborations have measured the *CP* parameter $\sin 2\beta$, where $\beta \equiv \arg[-V_{cd}V_{cb}^*/V_{td}V_{tb}^*]$, in $b \to (c\bar{c})s$ processes.

The leading-order diagrams contributing to $B^0 \to D^{(*)+}D^{(*)-}$ decays are shown in Fig. 1, where the color-favored tree-diagram of Fig. 1(a) dominates. When neglecting the penguin (loop) amplitude in Fig. 1(b), the mixing-induced *CP* asymmetry of $B^0 \to D^{(*)+}D^{(*)-}$, denoted *S*, is also determined by $\sin 2\beta$ [5]. The effect of neglecting the penguin amplitude has been estimated in models based on factorization and heavy quark symmetry, and the corrections are expected to be a few percent [6,7]. Large deviations of *S* in $B^0 \to D^{(*)+}D^{(*)-}$ decays with respect to $\sin 2\beta$ determined from $b \to (c\bar{c})s$ transitions could indicate physics beyond the SM [8–10].

The *CP* asymmetries of $B^0 \to D^{(*)+}D^{(*)-}$ decays have been studied by both the *BABAR* [11,12] and Belle [13–15] collaborations. In the SM, the direct *CP* asymmetry *C*, defined in Sec. IV, for the $B^0 \to D^{(*)+}D^{(*)-}$ decays is expected to be near zero. The Belle Collaboration has observed a 3.2 sigma deviation of *C* from zero in the $B^0 \to D^+D^-$ channel [15]. This has not been observed by *BABAR* nor has it been seen in other $B^0 \to D^{(*)+}D^{(*)-}$ decay modes, which involve the same quark-level diagrams. As was pointed out in [9], understanding any possible asymmetries in these decays is important to constraining theoretical models.

In this article, we update the previous measurements of *CP* asymmetry parameters in $B^0 \to D^{(*)+}D^{(*)-}$ decays [11,12], including the *CP*-odd fraction for $B^0 \to D^{*+}D^{*-}$, using the final *BABAR* data sample. Charge conjugate decays are included implicitly in expressions throughout this article unless otherwise indicated.

II. DETECTOR, DATA SAMPLE, AND RECONSTRUCTION

A. The *BABAR* detector

The data used in this analysis were collected with the *BABAR* detector [16] operating at the PEP-II *B* Factory located at the Stanford Linear Accelerator Center (SLAC). The *BABAR* dataset comprises $(467 \pm 5) \times 10^6$ $B\bar{B}$ pairs collected from 1999 to 2007 at the center-of-mass (CM) energy $\sqrt{s} = 10.58$ GeV, corresponding to the $\Upsilon(4S)$ resonance. We use GEANT4-based [17] Monte Carlo (MC)

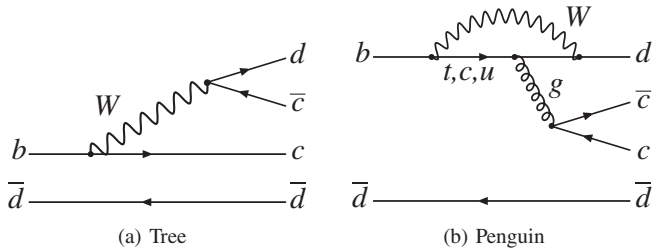

FIG. 1. Leading-order Feynman graphs for the $\bar{B}^0 \to D^{(*)+}D^{(*)-}$ decays.

simulation to study backgrounds and to validate the analysis procedures.

The asymmetric energies of the PEP-II beams provide an ideal environment to study time-dependent *CP* phenomena in the $B^0 - \bar{B}^0$ system by boosting the $\Upsilon(4S)$ in the laboratory frame, thus making possible precise determination of the decay vertices of the two B meson daughters. *BABAR* employs a five-layer silicon vertex tracker (SVT) close to the interaction region to provide precise vertex measurements and to track low momentum charged particles. A drift chamber (DCH) provides excellent momentum measurement of charged particles. Particle identification of kaons and pions is primarily derived from ionization losses in the SVT and DCH and from measurements of photons produced in the fused silica bars of a ring-imaging Cherenkov light detector (DIRC). A CsI(Tl) crystal-based electromagnetic calorimeter enables reconstruction of photons and identification of electrons. All of these systems operate within a 1.5 T superconducting solenoid, whose iron flux return is instrumented to detect muons.

B. Candidate reconstruction and selection

The candidates used in this analysis are formed from oppositely charged $D^{(*)}$ mesons where we include the D^{*+} decay modes $D^{*+} \to D^0\pi^+$ and $D^{*+} \to D^+\pi^0$ and D decay modes $D^0 \to K^-\pi^+$, $D^0 \to K^-\pi^+\pi^0$, $D^0 \to K^-\pi^+\pi^-\pi^+$, $D^0 \to K^0_S\pi^+\pi^-$, and $D^+ \to K^-\pi^+\pi^+$. In the $B^0 \to D^{*+}D^{*-}$ mode, we reject B^0 candidates where both D^* mesons decay to $D\pi^0$ because of its smaller branching fraction and larger backgrounds. Reference [18] contains the details of the reconstruction procedure, outlined here, used to select signal candidates. Charged kaon candidates must be identified as such using a likelihood technique based on the opening angle of the Cherenkov light measured in the DIRC and the ionization energy loss measured in the SVT and DCH [16]. We reconstruct K^0_S candidates from two oppositely charged tracks, geometrically constrained to a common vertex and with an invariant mass within 20 MeV of the nominal value [19]. We also require that the χ^2 probability of the vertex fit of the K^0_S be greater than 0.1%. We form π^0 candidates from a pair of photons detected in the calorimeter, each with energy greater than 40 MeV. The invariant mass of the two photons must be less than 30 MeV/c^2 from the nominal π^0 mass, and their summed energy must be greater than 200 MeV. In addition, we apply a mass constraint to the π^0 candidates. We require the reconstructed D meson candidate mass to be within 20 MeV/c^2 of the nominal value, except for the $D^0 \to K^-\pi^+\pi^0$ decays where we use a looser requirement of 40 MeV/c^2. The daughters of each D candidate are fit to a common vertex with their combined mass constrained to that of the D meson. We use D candidates combined with a pion track with momentum less than 450 MeV/c in the CM frame to form D^{*+} candidates. We fit the B^0 decay with a vertex constraint.

Since the time of our previous publications [11,12,18], the *BABAR* reconstruction routines have been extensively revised, leading to significant improvements in localizing and reconstructing tracks, particularly for low momentum charged particles. These improvements have increased the reconstruction efficiency for final states with multiple slow particles, such as the $B^0 \to D^{*+}D^{*-}$ channel which has a better than 20% improvement. As a result, the statistical sensitivity of the measurements in this paper has increased more than would be expected by just the increment in luminosity.

To suppress $e^+e^- \to q\bar{q}$ ($q = u$, d, s, and c) continuum background, we exploit the spherical shape of $B\bar{B}$ events by requiring the ratio of second to zeroth order Fox-Wolfram moments [20] to be less than 0.6. We select the B^0 candidates based on four variables: $\Delta E \equiv E^*_B - \sqrt{s}/2$, where E^*_B is the energy of the B meson in the CM frame, the D candidate flight length significance, defined as the sum of the two D candidate flight lengths divided by the error on the sum, a Fisher discriminant [21], and a mass likelihood of the $D^{(*)}$ mesons. The Fisher discriminant is a linear combination of 11 variables: the momentum flow in nine concentric cones around the thrust axis of the B^0 candidate, the angle between the thrust axis and the beam axis, and the angle between the line-of-flight of the B^0 candidate and the beam axis. The mass likelihood is formed from Gaussian functions,

$$\begin{aligned}\mathcal{L}_{\rm mass} = {} & G(m_D; m_{D_{\rm PDG}}, \sigma_{m_D}) \times G(m_{\bar{D}}; m_{\bar{D}_{\rm PDG}}, \sigma_{m_{\bar{D}}}) \\ & \times [f_{\rm core} G(\Delta m_{D^{*+}}; \Delta m_{D^{*+}_{\rm PDG}}, \sigma_{\Delta m_{\rm core}}) \\ & + (1 - f_{\rm core}) G(\Delta m_{D^{*+}}; \Delta m_{D^{*+}_{\rm PDG}}, \sigma_{\Delta m_{\rm tail}})] \\ & \times [f_{\rm core} G(\Delta m_{D^{*-}}; \Delta m_{D^{*-}_{\rm PDG}}, \sigma_{\Delta m_{\rm core}}) \\ & + (1 - f_{\rm core}) G(\Delta m_{D^{*-}}; \Delta m_{D^{*-}_{\rm PDG}}, \sigma_{\Delta m_{\rm tail}})], \end{aligned} \quad (1)$$

where the PDG subscript refers to the nominal value [22]. The reconstructed masses and uncertainties $\sigma_{m_{\bar{D}}}$ for the D mesons prior to the mass constraint are used in the likelihood. The D^* portion of the likelihood is the sum of two Gaussian functions, a central core and a wider tail. The value of $f_{\rm core}$ and the widths of the D^* Gaussian functions are taken from detailed signal MC studies, which show good agreement between data and MC samples. The selection criteria are optimized for each D decay channel to maximize the total signal significance $S/\sqrt{S+B}$ for each B^0 decay mode, where S and B are the signal and background yields, respectively. The optimized selections are specified in [18]. We keep candidates with $m_{\rm ES} \equiv \sqrt{s/4 - p^{*2}_B} > 5.23$ GeV/c^2, where p^*_B is the momentum of the B candidate in the CM frame. On average 1.1–1.8 candidates per event satisfy all of the selection criteria

depending on the process. When more than one B^0 candidate meets the selection criteria, the one with the best $\mathcal{L}_{\rm mass}$ is kept. We find from MC that this procedure retains the correct candidate more than 95% of the time.

To determine the signal yields of the data sample, we use unbinned maximum likelihood (ML) fits to the $m_{\rm ES}$ distributions. The signal is described by a Gaussian function and the combinatorial background by a threshold function [23]. In detailed MC studies of the background, we find that there is a background contribution that exceeds the threshold function in the region $m_{\rm ES} > 5.27\ {\rm GeV}/c^2$, where most of the signal events lie. We describe this component with a Gaussian function having the same mean and width as the signal and refer to it as peaking background because if neglected, it would lead to an overestimate of the signal yields. In the $B^0 \to D^{*+}D^{*-}$ channel, the peaking background arises primarily from misreconstructed $B^+ \to D^{*+}\bar{D}^{*0}$ events where the slow π^0 from the $\bar{D}^{*0} \to \bar{D}^0\pi^0$ decay is replaced by a π^- to form a D^{*-} candidate. For the other three processes, our studies of the composition of the peaking background show it to be consistent with that of the combinatorial background in the region $m_{\rm ES} < 5.27\ {\rm GeV}/c^2$. We treat the peaking background component as an extension of the combinatorial background. The peaking background yields relative to the signal are fixed from MC to $(1.6 \pm 1.9)\%$, $(7.1 \pm 5.9)\%$, and $(7.4 \pm 2.9)\%$ for the $B^0 \to D^{*+}D^{*-}$, $B^0 \to D^+D^-$, and $B^0 \to D^{*\pm}D^{\mp}$ modes, respectively, where the errors are due primarily to the size of the MC sample available for background studies. The signal mean and background shape are free parameters in the fits. We fix the width of the signal Gaussian shape for $B^0 \to D^+D^-$ and $B^0 \to D^{*\pm}D^{\mp}$ to 2.46 MeV$/c^2$ and 2.55 MeV$/c^2$, respectively, determined from MC, while the width of the $B^0 \to D^{*+}D^{*-}$ signal is allowed to float because of its much higher purity. The signal yields are 934 ± 40 $B^0 \to D^{*+}D^{*-}$ events, 152 ± 17 $B^0 \to D^+D^-$ events, 365 ± 26 $B^0 \to D^{*+}D^-$ events, and 359 ± 26 $B^0 \to D^+D^{*-}$ events, where the uncertainty is statistical only. The signal yields are consistent with previously measured $B^0 \to D^{(*)+}D^{(*)-}$ decay branching fractions from *BABAR* [18] and Belle [15,24]. When compared with past *BABAR* measurements

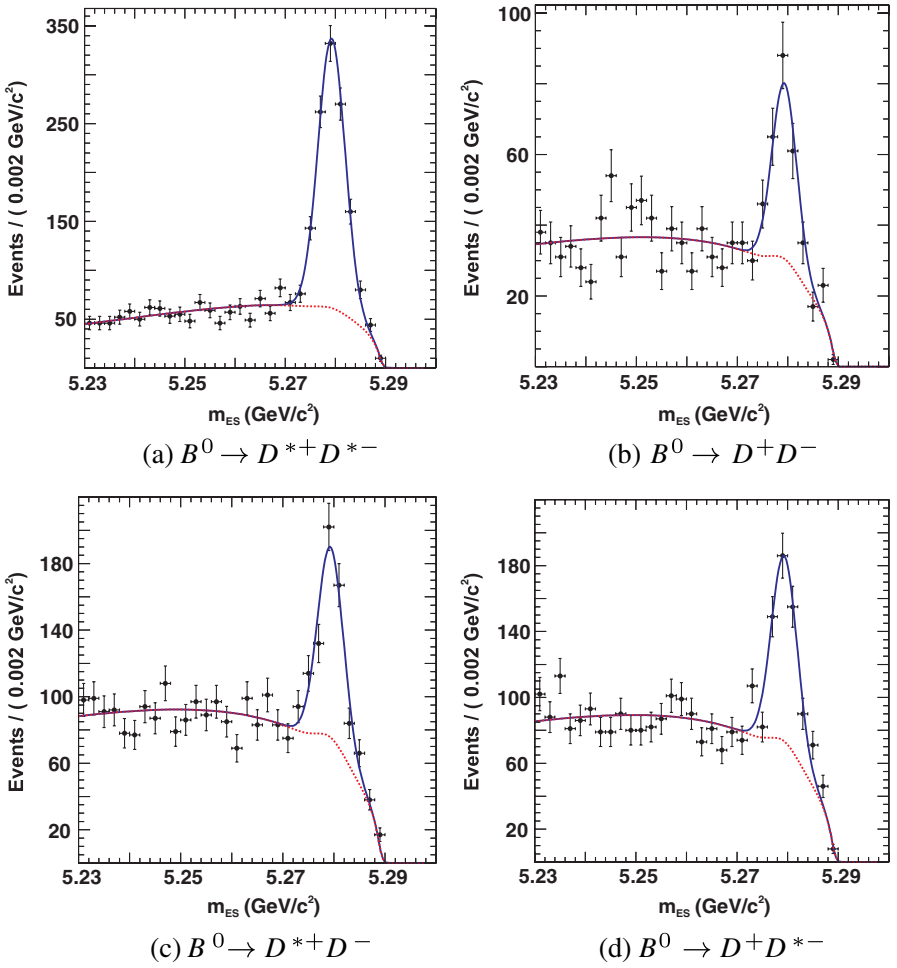

FIG. 2 (color online). Projections of the $m_{\rm ES}$ fit results. The solid line represents the total fit PDF and the dashed line is the background contribution.

[18,25,26], the low $B^0 \to D^+ D^{*-}$ yield in Ref. [11] is consistent with a statistical fluctuation. The fit projections for each mode onto $m_{\rm ES}$ are shown in Fig. 2.

III. TIME-INTEGRATED MEASUREMENT OF THE *CP*-ODD FRACTION

The $B^0 \to D^{*+} D^{*-}$ process has two vector mesons in the final state and is an admixture of *CP*-even and *CP*-odd states depending on the orbital angular momentum of the decay products. We measure the *CP*-odd fraction $R_\perp$ using a time-integrated angular analysis [27]. We define the three angles in the transversity basis as depicted in Fig. 3: the angle θ_1 between the slow pion from the D^{*-} and the direction opposite to the D^{*+} momentum in the D^{*-} rest frame; the polar angle $\theta_{\rm tr}$ and the azimuthal angle $\phi_{\rm tr}$ of the slow pion from the D^{*+} in the D^{*+} rest frame where the z axis is normal to the D^{*-} decay plane and the x axis is opposite the D^{*-} momentum. Working in the transversity basis, the time-dependent angular distribution of the B^0 decay products is

$$\frac{1}{\Gamma}\frac{d^4\Gamma}{d\cos\theta_1 d\cos\theta_{\rm tr} d\phi_{\rm tr} dt} = \frac{9}{16\pi}\frac{1}{|A_0|^2+|A_\parallel|^2+|A_\perp|^2}\Big\{2\cos^2\theta_1\sin^2\theta_{\rm tr}\cos^2\phi_{\rm tr}|A_0|^2 + \sin^2\theta_1\sin^2\theta_{\rm tr}\sin^2\phi_{\rm tr}|A_\parallel|^2$$
$$+ \sin^2\theta_1\cos^2\theta_{\rm tr}|A_\perp|^2 - \sin^2\theta_1\,\sin 2\theta_{\rm tr}\,\sin\phi_{\rm tr}\,{\rm Im}(A_\parallel^* A_\perp) + \frac{1}{\sqrt{2}}\sin 2\theta_1\sin^2\theta_{\rm tr}\,\sin 2\phi_{\rm tr}\,{\rm Re}(A_0^* A_\parallel)$$
$$- \frac{1}{\sqrt{2}}\sin 2\theta_1\,\sin 2\theta_{\rm tr}\cos\phi_{\rm tr}\,{\rm Im}(A_0^* A_\perp)\Big\}, \qquad (2)$$

where A_k, with $k = \parallel, 0, \perp$, represent time-dependent amplitudes given by

$$A_k(t) = \frac{\sqrt{2}A_k(0)}{1+|\lambda_k|^2}e^{-imt}e^{-t/2\tau_{B^0}}\left(\cos\frac{\Delta m_d t}{2} + i\eta_{CP}^k\lambda_k\sin\frac{\Delta m_d t}{2}\right). \qquad (3)$$

Here, η_{CP}^k is the *CP* eigenvalue, $+1$ for $A_{\parallel,0}$, -1 for $A_\perp$; λ_k is the *CP* parameter defined in Sec. IV; Δm_d is the B^0 mixing frequency, (0.507 ± 0.005) ps^{-1}; and τ_{B^0} is the B^0 lifetime, (1.530 ± 0.009) ps [19]. Expressions similar to Eq. (2) hold for $\bar{B}^0$ decays where each A_k is replaced by the appropriate $\bar{A}_k$ including $A_\perp \to -\bar{A}_\perp$. Integrating Eq. (2) over t, $\phi_{\rm tr}$, $\cos\theta_1$ and averaging over B flavor while taking into account detector efficiency yields

$$\frac{1}{\Gamma}\frac{d\Gamma}{d\cos\theta_{\rm tr}} = \frac{9}{32\pi}(1-R_\perp)\sin^2\theta_{\rm tr}\left\{\frac{1+\alpha}{2}I_0(\cos\theta_{\rm tr}) + \frac{1-\alpha}{2}I_\parallel(\cos\theta_{\rm tr})\right\} + \frac{3}{2}R_\perp\cos^2\theta_{\rm tr}\times I_\perp(\cos\theta_{\rm tr}), \qquad (4)$$

where we define

$$R_\perp = \frac{|A_\perp^0|^2}{|A_0^0|^2+|A_\parallel^0|^2+|A_\perp^0|^2} \qquad \alpha = \frac{|A_0^0|^2-|A_\parallel^0|^2}{|A_0^0|^2+|A_\parallel^0|^2},$$

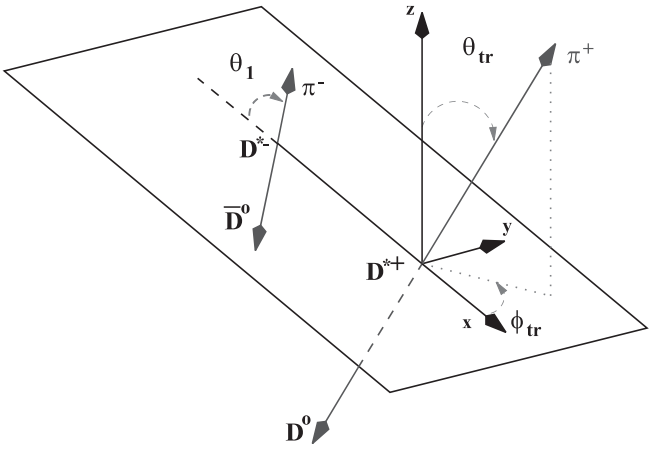

FIG. 3. Depiction of the $B^0 \to D^{*+} D^{*-}$ decay in the transversity basis with the $D^{*-} \to \bar{D}^0\pi^-$ decay plane shown. The three transversity angles are defined in the text.

and $A_k^0 = A_k(0)$. The three efficiency moments $I_k(\cos\theta_{\rm tr})$ are defined as

$$I_k(\cos\theta_{\rm tr}) = \int d\cos\theta_1 d\phi_{\rm tr} g_k(\theta_1, \phi_{\rm tr})\varepsilon(\theta_1, \theta_{\rm tr}, \phi_{\rm tr}), \qquad (5)$$

where $g_0 = 4\cos^2\theta_1\cos^2\phi_{\rm tr}$, $g_\parallel = 2\sin^2\theta_1\sin^2\phi_{\rm tr}$, $g_\perp = \sin^2\theta_1$, and ε is the detector efficiency. The moments I_k are parameterized as second-order even polynomials in $\cos\theta_{\rm tr}$ whose parameters are determined from signal MC simulation and fixed in the fit. The three I_k functions deviate only slightly from the same constant, making Eq. (4) nearly insensitive to α, which we fix to zero in the fit.

Because $\cos\theta_{\rm tr}$ is defined with respect to the slow pion from the D^{*+} decay, the measurement resolution smears its distribution. We convolve the function from Eq. (4) with a resolution function $\mathcal{R}(\Delta\theta_{\rm tr})$ which is modeled as the sum of three Gaussian functions. In addition, we include an uncorrelated Gaussian shape centered at $\pi/2$ and normalized in $0 < \theta_{\rm tr} < \pi$ to describe decays where the slow pion is poorly reconstructed leading to a loss of angular information. The uncorrelated term represents 3% of the signal events where both slow pions are charged and around 16%

in the modes where one of the slow pions is neutral. We determine the parameters of the resolution model and of the uncorrelated term from signal MC simulation and fix them in the ML fit. Small differences observed in the angular distributions based on the charge of the slow pions lead us to divide the efficiency moment and resolution parameters into three categories, $\pi^0\pi^-$, $\pi^+\pi^0$, and $\pi^+\pi^-$.

We determine $R_\perp$ in a simultaneous unbinned ML fit to the $m_{\rm ES}$ and $\cos\theta_{\rm tr}$ distributions for the three slow-pion modes. The $m_{\rm ES}$ probability density function (PDF) was described in Sec. II B. The signal $\cos\theta_{\rm tr}$ distribution is given by Eq. (4) convolved with the resolution model. The background $\cos\theta_{\rm tr}$ distribution is modeled as a second-order even polynomial $f_{\rm bg}(\cos\theta_{\rm tr}) = 1 + b_2\cos^2\theta_{\rm tr}$, where b_2, common to the three slow-pion modes, is allowed to float. The yield for each of the three slow-pion modes is determined by the fit. We validate the fitting procedure using high-statistics MC samples divided into data-sized subsets and find no significant bias. Fitting the data and including systematic uncertainties described below, we find

$$R_\perp = 0.158 \pm 0.028(\text{stat}) \pm 0.006(\text{syst}). \quad (6)$$

Figure 4 shows the projection of the fit result.

To evaluate the systematic uncertainty of $R_\perp$, we vary the parameters used to model the efficiency moments within the uncertainties of the MC simulation used to extract them. We do the same for the parameters used to model the experimental resolution. In both cases, we take into account correlations among the parameters when perturbing the values. We fix α to zero in the nominal fit, so we also set it to ± 1 and assign the effect on the fitted result as a systematic uncertainty. We change the $m_{\rm ES}$ and $\cos\theta_{\rm tr}$ shapes of the peaking background and assign the corresponding changes in $R_\perp$ as a systematic uncertainty. We allow the $\cos\theta_{\rm tr}$ background to have an additional fourth-order term to test our assumption of this background shape. This term is found to be consistent with zero, and we take the difference in $R_\perp$ with respect to the nominal second-order background description as the uncertainty with this model. We include as a systematic uncertainty the statistical uncertainty associated with the MC validation. A summary of the systematic uncertainties is found in Table I. The total systematic uncertainty is the sum in quadrature of the individual contributions.

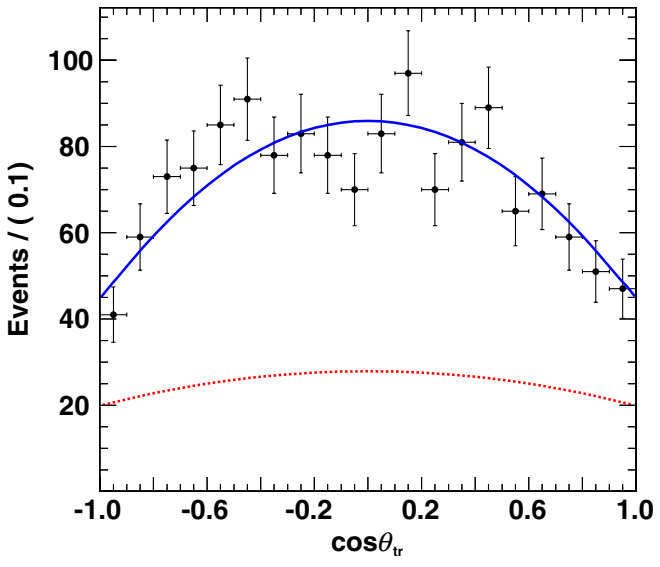

FIG. 4 (color online). Projection of the fit result onto $\cos\theta_{\rm tr}$ for events with $m_{\rm ES} > 5.27\text{GeV}/c^2$. The solid line is the projected fit result. The dashed line is the background component.

TABLE I. Summary of systematic uncertainties on the measurement of $R_\perp$.

Angular efficiency moments	0.0024
Angular measurement resolution	0.0036
α parameter uncertainty	0.0026
Peaking background	0.0014
$\cos\theta_{\rm tr}$ background shape	0.0002
Potential fit bias	0.0017
Total	0.0055

IV. TIME-DEPENDENT *CP* MEASUREMENT

The decay rate f_+ (f_-) of the neutral B meson to a common final state accompanied by a B^0 ($\bar{B}^0$) tag is

$$f_\pm(\Delta t) \propto e^{-|\Delta t|/\tau_{B^0}}\{(1 \mp \Delta w) \pm (1 - 2w) \times [S\sin(\Delta m_d \Delta t) - C\cos(\Delta m_d \Delta t)]\}, \quad (7)$$

with CP asymmetry parameters $S = 2\,\text{Im}(\lambda)/(1 + |\lambda|^2)$, $C = (1 - |\lambda|^2)/(1 + |\lambda|^2)$, and $\lambda = (q/p)(\bar{A}/A)$, where A ($\bar{A}$) is the decay amplitude for B^0 ($\bar{B}^0$) and q/p is the ratio of the flavor contributions to the mass eigenstates [28]. The parameter w is the average mistag probability, and Δw is the difference between the mistag probabilities for B^0 and $\bar{B}^0$. Here, $\Delta t \equiv t_{\rm reco} - t_{\rm tag}$ is the proper time difference between the B reconstructed as $B^0 \to D^{(*)+}D^{(*)-}$ ($B_{\rm rec}$) and the B used to tag the flavor ($B_{\rm tag}$). In the case of $B^0 \to D^{*+}D^{*-}$, we obtain an expression similar to Eq. (7) from Eqs. (2) and (3),

$$f_\pm(\Delta t, \cos\theta_{\rm tr}) \propto e^{-|\Delta t|/\tau_{B^0}}\{F(1 \mp \Delta w) \pm (1 - 2w) \times [G\sin(\Delta m_d \Delta t) - H\cos(\Delta m_d \Delta t)]\}. \quad (8)$$

The F, G, and H coefficients [29] are

$$\begin{aligned} F &= (1 - R_\perp)\sin^2\theta_{\rm tr} + 2R_\perp\cos^2\theta_{\rm tr}, \\ G &= (1 - R_\perp)S_+\sin^2\theta_{\rm tr} - 2R_\perp S_\perp\cos^2\theta_{\rm tr}, \\ H &= (1 - R_\perp)C_+\sin^2\theta_{\rm tr} + 2R_\perp C_\perp\cos^2\theta_{\rm tr}. \end{aligned} \quad (9)$$

The λ_k parameters in Eq. (3) need not be the same because

of possible differences in the relative contribution of penguin and tree amplitudes, therefore the S and C parameters for each of the three $(0, \|, \perp)$ amplitudes can also differ. Note that the minus sign before $S_\perp$ in the expression for G absorbs $\eta_{CP}^{\perp}$. We then define

$$S_+ = \frac{S_\| A_\|^{02} + S_0 A_0^{02}}{A_\|^{02} + A_0^{02}}, \qquad C_+ = \frac{C_\| A_\|^{02} + C_0 A_0^{02}}{A_\|^{02} + A_0^{02}}, \quad (10)$$

where $A_k^0 = A_k(0)$ from Eq. (3).

In the absence of penguin contributions, $S_{D^+D^-} = S_+ = S_\perp = -\sin 2\beta$, and $C_{D^+D^-} = C_+ = C_\perp = 0$. Because $B^0 \to D^{*\pm}D^{\mp}$ is not a CP eigenstate, the expressions for S and C are related, $S_{D^{*\pm}D^{\mp}} = -\sqrt{1 - C_{D^{*\pm}D^{\mp}}}\sin(2\beta_{\rm eff} \pm \delta)$, where δ is the strong phase difference between $B^0 \to D^{*+}D^-$ and $B^0 \to D^+D^{*-}$ decays [30]. Neglecting the penguin contributions, $\beta_{\rm eff} = \beta$, and $C_{D^{*+}D^-} = -C_{D^+D^{*-}}$.

The technique used to measure the time-dependent CP asymmetry is discussed in detail in Ref. [31]. We calculate Δt between the two B decays from the measured separation Δz of their decay vertices along the z axis. The $B_{\rm rec}$ decay vertex is determined from the daughter tracks of the $B^0 \to D^{(*)+}D^{(*)-}$ decay. The $B_{\rm tag}$ decay vertex is determined in a fit of the charged tracks not belonging to $B_{\rm rec}$ to a common vertex with a constraint on the beam spot location and the $B_{\rm rec}$ momentum. Events that do not satisfy $|\Delta t| < 20$ ps and $\sigma_{\Delta t} < 2.5$ ps are considered untagged in the time-dependent fit.

The flavor of the $B_{\rm tag}$ meson is determined using a multivariate analysis of its decay products [31]. The tagging algorithm classifies the B flavor and assigns the candidate to one of six mutually exclusive tagging categories based on the output. A seventh untagged category is for events where the flavor could not be determined. The performance of the tagging algorithm, its efficiency and mistag rates, is evaluated using the time-dependent evolution of a high-statistics data sample of $\Upsilon(4S) \to B_{\rm tag}B_{\rm flav}$, where the $B_{\rm flav}$ meson decays to a flavor eigenstate $D^{(*)-}h^+$ and h^+ may be a π^+, ρ^+, or a_1^+. The tagging algorithm has an efficiency $\varepsilon_{\rm tag} = (74.4 \pm 0.1)\%$ and an effective tagging power $Q \equiv \varepsilon_{\rm tag}(1-w)^2 = (31.2 \pm 0.3)\%$. The finite resolution of the B vertex reconstruction smears the distributions described in Eqs. (7) and (8). This measurement resolution is modeled as the sum of three Gaussian functions described in Ref. [31], the parameters of which are also determined from the $B_{\rm flav}$ sample.

We determine the CP asymmetry parameters in unbinned ML fits to the $m_{\rm ES}$, Δt, and in the case of $B^0 \to D^{*+}D^{*-}$, $\cos\theta_{\rm tr}$ distributions. The Δt signal distributions are given in Eqs. (7) and (8) convolved with the experimental resolution. The Δt background distribution has both zero and nonzero lifetime components which are convolved with the experimental resolution. The lifetime component is allowed to have effective CP parameters and lifetime, which are determined in the fits. The angular measurement resolution, determined for the CP-odd fraction measurement, is convolved with the signal angular distribution. The efficiency moments are not modeled but rather absorbed into an effective $R_\perp$, which is determined in the fit. This procedure simplifies the $\cos\theta_{\rm tr}$ distribution and does not introduce a bias. The peaking background for the $B^0 \to D^{(*)\pm}D^{\mp}$ channels shares the Δt background distributions with the combinatorial background because it originates from similar sources. The $B^0 \to D^{*+}D^{*-}$ peaking background has only a lifetime component, since it originates from a specific B^+ decay. Untagged events are also included in the fits to constrain the $m_{\rm ES}$ and $\cos\theta_{\rm tr}$ shapes but do not contribute to the determination of the CP parameters. We also allow the signal yield, the $m_{\rm ES}$ background shape, and the $\cos\theta_{\rm tr}$ background shape to vary in the fits. Again we use high-statistics MC samples divided into data-sized subsets to validate the fitting procedure and find no significant bias.

The statistical uncertainties of the CP measurements below are consistent with the expected uncertainties obtained from MC studies that include the signal and background yields observed in data. The statistical uncertainty for the $B^0 \to D^{(*)\pm}D^{\mp}$ channels is essentially unchanged or even slightly worse than our previous measurement [11]. We interpret this as a downward fluctuation in the statistical uncertainty of the previous measurement. Using MC data, we estimate the probability of observing such a fluctuation at about 20%. For each measurement that follows, the first uncertainty is statistical and the second is systematic.

From the fit to the $B^0 \to D^{*+}D^{*-}$ data, we find

$$\begin{aligned} S_+ &= -0.76 \pm 0.16 \pm 0.04 \\ C_+ &= +0.00 \pm 0.12 \pm 0.02 \\ S_\perp &= -1.80 \pm 0.70 \pm 0.16 \\ C_\perp &= +0.41 \pm 0.49 \pm 0.08, \end{aligned} \quad (11)$$

with an effective $R_\perp = 0.155 \pm 0.030$. If we perform the fit with the additional constraints that $S_+ = S_\perp = S_{D^{*+}D^{*-}}$ and $C_+ = C_\perp = C_{D^{*+}D^{*-}}$, we obtain

$$\begin{aligned} S_{D^{*+}D^{*-}} &= -0.70 \pm 0.16 \pm 0.03 \\ C_{D^{*+}D^{*-}} &= +0.05 \pm 0.09 \pm 0.02, \end{aligned} \quad (12)$$

having an effective $R_\perp = 0.171 \pm 0.028$. Fitting the $B^0 \to D^+D^-$ data yields

$$\begin{aligned} S_{D^+D^-} &= -0.63 \pm 0.36 \pm 0.05 \\ C_{D^+D^-} &= -0.07 \pm 0.23 \pm 0.03, \end{aligned} \quad (13)$$

and fitting the $B^0 \to D^{*\pm}D^{\mp}$ data yields

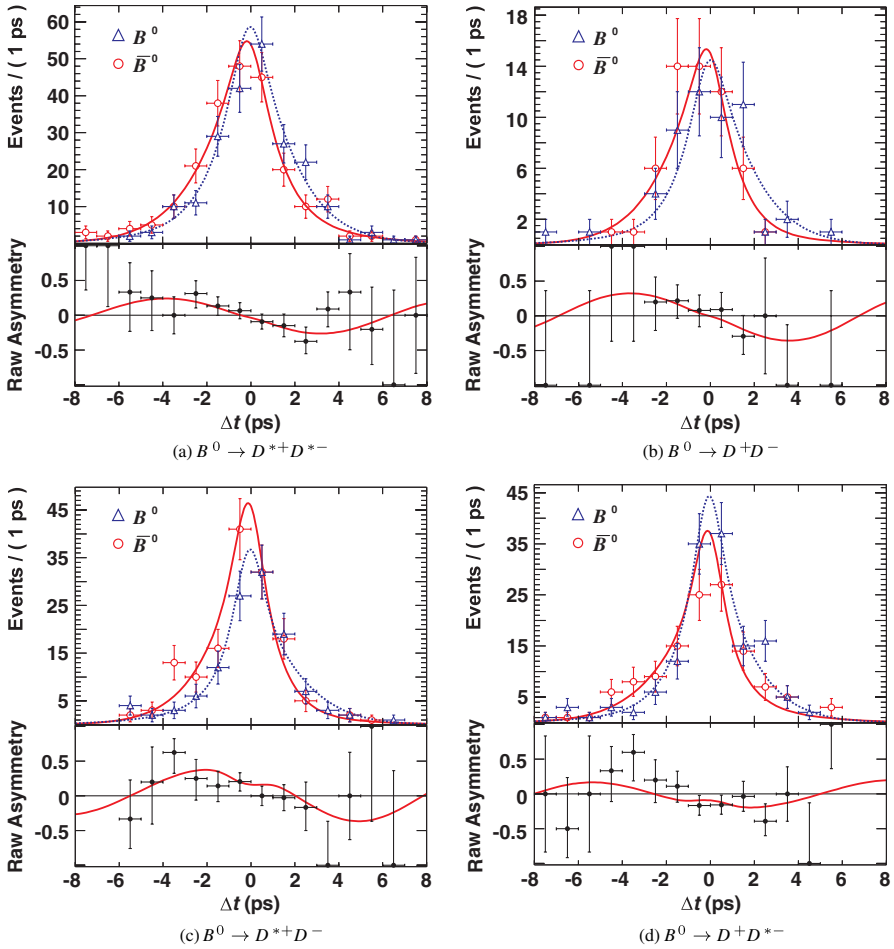

FIG. 5 (color online). Projections onto Δt of the fit result and the data in the region $m_{\rm ES} > 5.27$ GeV/c^2 for the three highest purity tagging categories. The triangular points and the dashed lines are for B^0 tagged events, and the circular points and solid lines are for $\bar{B}^0$ tagged events.

$$\begin{aligned} S_{D^{*+}D^-} &= -0.62 \pm 0.21 \pm 0.03 \\ S_{D^+D^{*-}} &= -0.73 \pm 0.23 \pm 0.05 \\ C_{D^{*+}D^-} &= +0.08 \pm 0.17 \pm 0.04 \\ C_{D^+D^{*-}} &= +0.00 \pm 0.17 \pm 0.03. \end{aligned} \tag{14}$$

Projections of the fit results onto Δt for events in the region $m_{\rm ES} > 5.27$ GeV/c^2, and their flavor asymmetry, can be seen in Fig. 5. To enhance the visibility of the signal in these projections, we use three of the six tagging categories with the highest purity, which account for 80% of the total effective tagging power Q. The correlations among the CP parameters are given in the appendix.

We evaluate systematic uncertainties in the CP asymmetries for each mode by varying the fixed parameters for the mistag quantities and Δt resolution model within their uncertainties while accounting for correlations among the parameters. For the $B^0 \to D^+D^-$ and $B^0 \to D^{*\pm}D^{\mp}$ modes, we change the fixed $m_{\rm ES}$ signal width by ± 0.2 MeV/c^2, an amount determined from a comparison of data and MC event samples in modes with high purity, and take the difference in fitted results as a systematic uncertainty. Additionally, we vary the fraction and shape of the peaking background component. We also include systematics for possible detector misalignment and the presence of doubly-Cabibbo suppressed decays of the $B_{\rm tag}$ meson [32]. We assign a systematic uncertainty equal to the statistical uncertainty of the MC sample used to validate the fit. Other sources of systematic uncertainty include: the B^0 meson properties (Δm_d and τ_{B^0}), which we vary to $\pm 1\sigma$ of their world averages, and uncertainty in the boost; the corresponding changes in the CP asymmetries are taken as the estimate of the systematic uncertainties. For the $B^0 \to D^{*+}D^{*-}$ mode, we vary the $\cos\theta_{\rm tr}$ resolution parameters and background shape in the manner described for the evaluation of systematic uncertainties on $R_\perp$ and take the effects on the CP parameters as the associated systematic uncertainty. A summary of the systematic uncertainties for the CP parameters is given in Tables II and III. As before, the total systematic uncertainty is the sum in quadrature of the individual contributions.

TABLE II. Systematic uncertainties on the $B^0 \to D^{*+}D^{*-}$ *CP* parameters.

	S_+	$S_\perp$	C_+	$C_\perp$	$S_{D^{*+}D^{*-}}$	$C_{D^{*+}D^{*-}}$
Tagging and Δt resolution	0.022	0.031	0.010	0.017	0.021	0.009
Peaking background	0.012	0.079	0.002	0.019	0.012	0.003
Detector Alignment	0.006	0.029	0.001	0.019	0.005	0.002
Doubly-Cabibbo suppressed decays	0.002	0.002	0.014	0.014	0.002	0.014
Potential Fit Bias	0.011	0.098	0.008	0.065	0.011	0.007
Angular PDF variations	0.025	0.091	0.004	0.015	0.011	0.001
Other	0.013	0.025	0.005	0.029	0.013	0.002
Total	0.040	0.163	0.020	0.080	0.032	0.018

TABLE III. Systematic uncertainties on the $B^0 \to D^{(*)\pm}D^{\mp}$ *CP* parameters.

	$S_{D^+D^-}$	$C_{D^+D^-}$	$S_{D^{*+}D^-}$	$C_{D^{*+}D^-}$	$S_{D^+D^{*-}}$	$C_{D^+D^{*-}}$
Tagging and Δt resolution	0.031	0.011	0.027	0.012	0.029	0.011
$m_{\rm ES}$ signal width	0.034	0.020	0.013	0.018	0.028	0.012
Peaking background	0.018	0.007	0.014	0.023	0.030	0.013
Detector alignment	0.002	0.001	0.004	0.002	0.002	0.001
Doubly-Cabibbo suppressed decays	0.002	0.014	0.002	0.014	0.002	0.014
Potential Fit Bias	0.007	0.005	0.008	0.006	0.008	0.006
Other	0.006	0.002	0.002	0.006	0.004	0.003
Total	0.051	0.028	0.034	0.036	0.051	0.026

Because $B^0 \to D^{*\pm}D^{\mp}$ decays are not *CP* eigenstates, it is illustrative to express the *CP* asymmetry parameters S and C in a slightly different parametrization [33]

$$\begin{aligned} S_{D^*D} &= \tfrac{1}{2}(S_{D^{*+}D^-} + S_{D^+D^{*-}}) \\ \Delta S_{D^*D} &= \tfrac{1}{2}(S_{D^{*+}D^-} - S_{D^+D^{*-}}) \\ C_{D^*D} &= \tfrac{1}{2}(C_{D^{*+}D^-} + C_{D^+D^{*-}}) \\ \Delta C_{D^*D} &= \tfrac{1}{2}(C_{D^{*+}D^-} - C_{D^+D^{*-}}). \end{aligned} \tag{15}$$

The S_{D^*D} and C_{D^*D} parameters characterize mixing-induced *CP* violation related to the angle β and flavor-dependent direct *CP* violation, respectively. ΔS_{D^*D} is insensitive to *CP* violation but is related to the strong phase difference δ. ΔC_{D^*D} describes the asymmetry between the rates $\Gamma(B^0 \to D^{*+}D^-) + \Gamma(\bar{B}^0 \to D^+D^{*-})$ and $\Gamma(B^0 \to D^+D^{*-}) + \Gamma(\bar{B}^0 \to D^{*+}D^-)$. Using the results from Eq. (14) and taking into account correlations among the variables, we find

$$\begin{aligned} S_{D^*D} &= -0.68 \pm 0.15 \pm 0.04 \\ \Delta S_{D^*D} &= +0.05 \pm 0.15 \pm 0.02 \\ C_{D^*D} &= +0.04 \pm 0.12 \pm 0.03 \\ \Delta C_{D^*D} &= +0.04 \pm 0.12 \pm 0.03. \end{aligned} \tag{16}$$

From the signal yields $N_{D^{*+}D^-}$ and $N_{D^+D^{*-}}$ determined in the time-dependent fit described above, we also measure the time-integrated *CP* asymmetry in $B^0 \to D^{*\pm}D^{\mp}$ decays, defined as

$$\mathcal{A} = \frac{N_{D^{*+}D^-} - N_{D^+D^{*-}}}{N_{D^{*+}D^-} + N_{D^+D^{*-}}}. \tag{17}$$

We find

$$\mathcal{A} = +0.008 \pm 0.048(\text{stat}) \pm 0.013(\text{syst}), \tag{18}$$

where the systematic uncertainty is dominated by track reconstruction efficiency differences for positive and negative tracks (0.013). There is also a small contribution from the $m_{\rm ES}$ signal width, peaking background, and MC statistics (0.002).

V. CONCLUSION

We have measured the *CP* asymmetry parameters for $B^0 \to D^{(*)+}D^{(*)-}$ decays, including the *CP*-odd fraction in the $B^0 \to D^{*+}D^{*-}$ channel, using the final *BABAR* data sample. All of the S parameters are consistent with the value of $\sin 2\beta$ measured in $b \to (c\bar{c})s$ transitions [34] and with the expectation from the standard model for small penguin contributions. The C parameters are consistent with zero in all modes. In particular, we see no evidence of the large direct *CP* violation reported by the Belle Collaboration in the $B^0 \to D^+D^-$ channel [15]. This measurement supersedes the previous *BABAR* measurements [11,12] of *CP* asymmetries in these decays.

ACKNOWLEDGMENTS

We are grateful for the extraordinary contributions of our PEP-II colleagues in achieving the excellent luminosity and machine conditions that have made this work possible. The success of this project also relies critically on the expertise and dedication of the computing organizations that support *BABAR*. The collaborating institutions wish to thank SLAC for its support and the kind hospitality extended to them. This work is supported by the U.S. Department of Energy and National Science Foundation, the Natural Sciences and Engineering Research Council (Canada), the Commissariat à l'Energie Atomique and Institut National de Physique Nucléaire et de Physique des Particules (France), the Bundesministerium für Bildung und Forschung and Deutsche Forschungsgemeinschaft (Germany), the Istituto Nazionale di Fisica Nucleare (Italy), the Foundation for Fundamental Research on Matter (The Netherlands), the Research Council of Norway, the Ministry of Education and Science of the Russian Federation, Ministerio de Educación y Ciencia (Spain), and the Science and Technology Facilities Council (United Kingdom). Individuals have received support from the Marie-Curie IEF program (European Union) and the A. P. Sloan Foundation.

APPENDIX: CORRELATIONS AMONG THE *CP* PARAMETERS

To allow detailed use of these results, we include the correlation matrices for the *CP* parameters. Table IV contains correlations among the fit parameters in the $B^0 \to D^{*+}D^{*-}$ channel with separate *CP*-even and *CP*-odd asymmetries, and in the combined case, the correlation between $S_{D^{*+}D^{*-}}$ and $C_{D^{*+}D^{*-}}$ is 0.8% with correlations to the effective $R_\perp$ the same as the *CP*-even parameters. Table V contains the correlations among the $B^0 \to D^{*\pm}D^{\mp}$ asymmetries. The correlation of the time-integrated *CP* asymmetry $\mathcal{A}$ with any of the *CP* parameters is less than 0.1%. The correlation between $S_{D^+D^-}$ and $C_{D^+D^-}$ is -1.2%.

TABLE IV. Correlations among the *CP* parameters of the $B^0 \to D^{*+}D^{*-}$ mode split by *CP*-even and *CP*-odd.

	S_+	C_+	$S_\perp$	$C_\perp$	$R_\perp$
S_+	1	0.008	0.376	−0.036	−0.083
C_+		1	0.045	−0.465	0.003
$S_\perp$			1	−0.224	0.471
$C_\perp$				1	−0.151
$R_\perp$					1

TABLE V. Correlations among the *CP* parameters of the $B^0 \to D^{*\pm}D^{\mp}$ mode.

	$S_{D^{*+}D^-}$	$C_{D^{*+}D^-}$	$S_{D^+D^{*-}}$	$C_{D^+D^{*-}}$
$S_{D^{*+}D^-}$	1	−0.039	0.002	0.001
$C_{D^{*+}D^-}$		1	−0.001	−0.001
$S_{D^+D^{*-}}$			1	−0.009
$C_{D^+D^{*-}}$				1

[1] N. Cabibbo, Phys. Rev. Lett. **10**, 531 (1963).
[2] M. Kobayashi and T. Maskawa, Prog. Theor. Phys. **49**, 652 (1973).
[3] B. Aubert *et al.* (*BABAR* Collaboration), Phys. Rev. Lett. **87**, 091801 (2001).
[4] K. Abe *et al.* (Belle Collaboration), Phys. Rev. Lett. **87**, 091802 (2001).
[5] A. I. Sanda and Z. Z. Xing, Phys. Rev. D **56**, 341 (1997).
[6] Z. Z. Xing, Phys. Lett. B **443**, 365 (1998).
[7] Z. Z. Xing, Phys. Rev. D **61**, 014010 (1999).
[8] Y. Grossman and M. P. Worah, Phys. Lett. B **395**, 241 (1997).
[9] M. Gronau, J. L. Rosner, and D. Pirjol, Phys. Rev. D **78**, 033011 (2008).
[10] R. Zwicky, Phys. Rev. D **77**, 036004 (2008).
[11] B. Aubert *et al.* (*BABAR* Collaboration), Phys. Rev. Lett. **99**, 071801 (2007).
[12] B. Aubert *et al.* (*BABAR* Collaboration), Phys. Rev. D **76**, 111102 (2007).
[13] H. Miyake *et al.* (Belle Collaboration), Phys. Lett. B **618**, 34 (2005).
[14] T. Aushev *et al.* (Belle Collaboration), Phys. Rev. Lett. **93**, 201802 (2004).
[15] S. Fratina *et al.* (Belle Collaboration), Phys. Rev. Lett. **98**, 221802 (2007).
[16] B. Aubert *et al.* (*BABAR* Collaboration), Nucl. Instrum. Methods Phys. Res., Sect. A **479**, 1 (2002).
[17] S. Agostinelli *et al.* (GEANT4 Collaboration), Nucl. Instrum. Methods Phys. Res., Sect. A **506**, 250 (2003).
[18] B. Aubert *et al.* (*BABAR* Collaboration), Phys. Rev. D **73**, 112004 (2006).
[19] W. M. Yao *et al.* (Particle Data Group), J. Phys. G **33**, 1 (2006).
[20] G. C. Fox and S. Wolfram, Phys. Rev. Lett. **41**, 1581 (1978).
[21] D. M. Asner *et al.* (CLEO Collaboration), Phys. Rev. D **53**, 1039 (1996).
[22] S. Eidelman *et al.* (Particle Data Group), Phys. Lett. B **592**, 1 (2004).
[23] H. Albrecht *et al.* (ARGUS Collaboration), Phys. Lett. B **241**, 278 (1990).

[24] K. Abe *et al.* (Belle Collaboration), Phys. Rev. Lett. **89**, 122001 (2002).
[25] B. Aubert *et al.* (*BABAR* Collaboration), Phys. Rev. Lett. **95**, 131802 (2005).
[26] B. Aubert *et al.* (*BABAR* Collaboration), Phys. Rev. Lett. **90**, 221801 (2003).
[27] I. Dunietz, H. R. Quinn, A. Snyder, W. Toki, and H. J. Lipkin, Phys. Rev. D **43**, 2193 (1991).
[28] P. F. Harrison and H. R. Quinn (*BABAR* Collaboration), Report No. SLAC-R-0504, 1998; *BABAR* Collaboration, Papers from Workshop on Physics at an Asymmetric *B* Factory, Rome, Italy, 1996, Princeton, NJ, 1997, Orsay, France, 1997 and Pasadena, CA, 1997.
[29] The order of the definition of these coefficients has changed since our previous publication [12].
[30] R. Aleksan, A. Le Yaouanc, L. Oliver, O. Pene, and J. C. Raynal, Phys. Lett. B **317**, 173 (1993).
[31] B. Aubert *et al.* (*BABAR* Collaboration), Phys. Rev. D **66**, 032003 (2002).
[32] O. Long, M. Baak, R. N. Cahn, and D. Kirkby, Phys. Rev. D **68**, 034010 (2003).
[33] B. Aubert *et al.* (*BABAR* Collaboration), Phys. Rev. Lett. **91**, 201802 (2003).
[34] B. Aubert *et al.* (*BABAR* Collaboration), Phys. Rev. Lett. **99**, 171803 (2007).